Effects of parity-time symmetry in nonlinear Klein-Gordon models and their stationary kinks

A. Demirkaya,[1] D. J. Frantzeskakis,[2] P. G. Kevrekidis,[3] A. Saxena,[4] and A. Stefanov[5]
[1]*Mathematics Department, University of Hartford, 200 Bloomeld Avenue, West Hartford, Connecticut 06112, USA*
[2]*Department of Physics, University of Athens, Panepistimiopolis, Zografos, Athens 15784, Greece*
[3]*Department of Mathematics and Statistics, University of Massachusetts, Amherst, Massachusetts 01003-4515, USA*
[4]*Center for Nonlinear Studies and Theoretical Division, Los Alamos National Laboratory, Los Alamos, New Mexico 87545, USA*
[5]*Department of Mathematics, University of Kansas, 1460 Jayhawk Blvd., Lawrence, Kansas 66045-7523, USA*
(Received 14 May 2013; published 12 August 2013)

In this work, we introduce some basic principles of $\mathcal{PT}$-symmetric Klein-Gordon nonlinear field theories. By formulating a particular antisymmetric gain and loss profile, we illustrate that the stationary states of the model do not change. However, the stability critically depends on the gain and loss profile. For a symmetrically placed solitary wave (in either the continuum model or a discrete analog of the nonlinear Klein-Gordon type), there is no effect on the steady state spectrum. However, for asymmetrically placed solutions, there exists a measurable effect of which a perturbative mathematical characterization is offered. It is generally found that asymmetry towards the lossy side leads towards stability, while towards the gain side produces instability. Furthermore, a host of finite size effects, which disappear in the infinite domain limit, are illustrated in connection to the continuous spectrum of the problem.

DOI: 10.1103/PhysRevE.88.023203 PACS number(s): 05.45.Yv

I. INTRODUCTION

Parity-time ($\mathcal{PT}$) symmetric settings have recently captured the fascination of both physicists and mathematicians working in linear and nonlinear systems alike. While the original proposal of Bender and co-workers involved a new framework for $\mathcal{PT}$-symmetric quantum mechanics [1–3], the prototypical implementation that arose about a decade later was in optics through the work of Christodoulides and co-workers [4–8]; see also the earlier linear work of [9]. The first realization of $\mathcal{PT}$ symmetry emerged in the so-called passive-$\mathcal{PT}$ setting, in which two wave guides, one with loss and the other without loss, were used [6]. A similar proposal, namely a leaky dimer, was formulated in the context of cold atom physics, and studied in the framework of the Bose-Hubbard model [10]. Subsequently, an optical wave-guide system with both gain and loss was experimentally studied [7]. Theoretical investigations have rapidly followed for such dimer-type settings [11–23] and generalizations thereof, including ones where the gain-loss contributions appear in a balanced form in front of the nonlinear term [24–27].

On the other hand, much less attention has been paid to another, yet quite intriguing, set of questions that emerge in the case of $\mathcal{PT}$-symmetric Klein-Gordon field theories [28,29]; the latter are of particular relevance to both mechanical systems (e.g., arrays of coupled pendula [29]) and electrical ones (e.g., electrical circuits with capacitive, inductive, and resistive elements [30]). At this point, it should be noted that there is an ongoing activity [31,32] towards utilizing, for example, controllable settings of electric circuits in order to showcase the principles of linear $\mathcal{PT}$-symmetric settings, such as the linear $\mathcal{PT}$ phase transition. Moreover, experimental efforts to produce a mechanical system featuring $\mathcal{PT}$ symmetry have recently been reported [33], as have theoretical proposals for nonlinear $\mathcal{PT}$-symmetric metamaterials and the formation of gain-driven discrete breathers therein [34]. Nevertheless, the literature on partial differential equations (PDEs) modeling $\mathcal{PT}$-symmetric Klein-Gordon systems is rather sparse; one of the very few field-theoretic examples of this sort can be found in Ref. [35] (which is in itself a model of mathematical interest rather than directly motivated from physics).

It is the purpose of this work to contribute to this very direction, by proposing and studying a Klein-Gordon model that, while not being Hamiltonian, respects the $\mathcal{PT}$ symmetry. The proposed model possesses gain and loss balancing through an odd function, and this feature is studied for the sine-Gordon (sG) and the ϕ^4 models [28,29], arguably two of the most famous field theoretic examples of nonlinear Klein-Gordon models. The gain and loss are introduced in a way that does not affect the steady states of the problem. Among such states, we select to study one of the prototypical kinds of relevance to the field theory, namely, the kinklike instanton structure, i.e., the heteroclinic orbit that connects two of the stable uniform states of the system. As a vehicle for our studies, we use the discrete analog of the PDE, namely, the nonlinear dynamical lattice which constitutes its discretization. This is of interest in its own right, not only due to the fundamental mathematical and physical features that arise therein (radiation, internal modes, Peierls-Nabarro barriers, etc. [36,37]), but also because the discrete model arises in experimentally relevant mechanical and electrical systems [31,32,38,39], including $\mathcal{PT}$-symmetric ones.

We argue that in the PDE the stability of the steady states should *not* be affected for suitably, symmetrically placed kinks between the gain and loss region. In the discrete problem, similar symmetric placement of the kink leads to a vanishing effect both for the even site case of intersite-centered kinks and for the odd site case of site-centered kinks. However, asymmetric placement of the kink with respect to the gain and loss interface may generate a destabilization effect. A perturbative analytical expression is provided that allows us to evaluate whether such a destabilization may occur. Furthermore, we provide a rigorous estimate that bounds the growth rate of any potential instability by an explicit numerical factor multiplying the order ϵ of the $\mathcal{PT}$-symmetric

perturbation. In our numerical computations, it is typically found that the kink is stabilized when moving towards the lossy side, while it is destabilized when moving towards the gain side. In addition, interesting finite size effects arise that disappear in the infinite lattice size limit.

Our presentation is organized as follows. In Sec. II, we present the overarching mathematical formalism, providing the model and the notion of $\mathcal{PT}$ symmetry in such Klein-Gordon settings. We also discuss the spectral stability analysis and its formulation, as well as a principal result based on the Fredholm alternative that enables us to compute $\mathcal{PT}$-symmetry induced bifurcations of eigenvalues and a rigorous estimate on the potential growth rate of the perturbations. In Sec. III, we analyze the results of numerical computations in the discrete problem; in particular, we systematically study intersite-centered and site-centered kinks in the discrete setting, for finite (and going towards infinite) lattices, and for discrete chains (and going towards continuum intervals or lines). Representative spectral results are also given for the ϕ^4 case to illustrate the generality of the conclusions; additionally, the spectral conclusions are corroborated by selected dynamical evolution computations. Finally, in Sec. IV, we briefly summarize our findings and present a number of possibilities for future studies.

II. MATHEMATICAL MODEL AND ANALYTICAL CONSIDERATIONS

In what follows, we will focus on partial differential equations of the form

$$u_{tt} - u_{xx} = f(u) + \gamma(x)u_t. \tag{1}$$

Here, subscripts denote partial derivatives, $f(u)$ is the nonlinear function that depends on the field u which, in turn, depends on the variables x and t, and $\gamma(x)$ is a function accounting for the presence of gain and loss in the system. For $\gamma = 0$, and for specific choices of $f(u)$, the system possesses topological solutions, in the form of kinks, that we will consider below. In particular, for the sine-Gordon field theory $f(u) = -\sin(u)$ and the prototypical kink solution that we will consider will be of the form $u(x) = 4\arctan(e^x)$. On the other hand, for the ϕ^4 model, $f(u) = 2(u - u^3)$, and the relevant kink assumes the form $u(x) = \tanh(x)$.

While the D'Alembertian (linear) operator $\partial_t^2 - \partial_x^2$ preserves the $\mathcal{PT}$ symmetry, this is not generically true in the case of the gain and loss term $\gamma(x)u_t$. Taking $t \to -t$ and $x \to -x$, and requiring that the system be identical under this transformation, leads to the immediate constraint that $\gamma(-x) = -\gamma(x)$, i.e., that the gain and loss profile should be odd. In what follows, we will use a localized gain and loss profile, namely, $\gamma(x) = \epsilon x e^{-x^2/2}$, where ϵ characterizes the strength of the relevant perturbation.

At this point, it is important to note that while the existence of other solutions such as traveling-wave solutions or breather solutions may be drastically affected by the presence of the $\mathcal{PT}$-symmetric gain and loss term, the static kink solutions are not affected and are, in fact, shared by the Hamiltonian and the $\mathcal{PT}$-symmetric variant of the model. We will defer considerations of other important solutions, such as the traveling waves and the breathers, to a future study. Here, we seek to understand the implications of the $\mathcal{PT}$-symmetric perturbation for the spectral stability of the kink solutions and their associated nonlinear dynamics. In that light, we will examine the fate of perturbations of steady solutions $u_0(x)$ in the form

$$u(x,t) = u_0(x) + \delta w(x)e^{\lambda t}. \tag{2}$$

It is then straightforward to infer that the eigenvalue-eigenvector pair $[\lambda, w(x)]$ will satisfy the linearization equation [to $O(\delta)$] of the form:

$$\lambda^2 w = w_{xx} + f'[u_0(x)]w + \gamma(x)\lambda w. \tag{3}$$

Interestingly, this gives rise to a quadratic operator pencil of the form

$$[\lambda^2 \hat{A} + \lambda \hat{B} + \hat{C}]w(x) = 0, \tag{4}$$

where $\hat{A}$ represents the identity operator, $\hat{B} = -\gamma(x)$ is a multiplicative operator incorporating the gain and loss profile, and $\hat{C} = -\partial_x^2 - f'(u_0)$, which for the purposes of the models that we consider here (and if we expect the Hamiltonian analog of the solution to be stable) will be a positive definite one. It should be noted that such quadratic pencils have been studied in the mathematical literature (see the example of [40]); however, this study has been limited to the simpler case where $\hat{C}$ is a negative definite operator, in which case the spectrum is significantly simpler.

Solving Eq. (4) as a linear eigenvalue problem is addressed in the following way. The problem is split into a first order one $u_t = p$, and writing Eq. (1) as $p_t = u_{xx} + f(u) + \gamma(x)p$. Then, using the decomposition $u(x,t) = u_0(x) + \delta w_1(x)e^{\lambda t}$ and $p(x,t) = \delta w_2(x)e^{\lambda t}$, we obtain the first order "augmented" eigenvalue problem of the form

$$\lambda \begin{pmatrix} w_1 \\ w_2 \end{pmatrix} = \begin{pmatrix} 0 & I \\ -\hat{C} & \gamma(x) \end{pmatrix} \begin{pmatrix} w_1 \\ w_2 \end{pmatrix}, \tag{5}$$

which can be solved directly as a matrix eigenvalue problem (upon suitable discretization).

Although Eq. (5) is more straightforward to use for numerical computations, let us use Eqs. (3) and (4) to develop some insight on the $\mathcal{PT}$-symmetry induced corrections to the stability problem. In particular, considering the case of a weak gain and loss term, with $\hat{B} = \epsilon \hat{B}_0$, we can employ a perturbation expansion of the form

$$\lambda = \lambda_0 + \epsilon\lambda_1 + \cdots, \tag{6}$$

$$w = w_0 + \epsilon w_1 + \cdots. \tag{7}$$

Then, to $O(\epsilon)$, this leads to the condition

$$(\lambda_0^2 + \hat{C})w_1 = \lambda_0(\hat{B}_0 - 2\lambda_1)w_0. \tag{8}$$

Upon applying the Fredholm alternative condition, i.e., by projecting to the kernel of the left-hand side, consisting of the eigenvectors w_0, Eq. (8) leads to the solvability condition that provides a correction to the eigenvalues, namely,

$$\lambda_1 = \frac{1}{2}\frac{\langle w_0, \hat{B}_0 w_0\rangle}{\langle w_0, w_0\rangle}. \tag{9}$$

$\langle .,. \rangle$ in Eq. (9) denotes the standard dot product. In the following, we will use this formula to evaluate the corrections

to the eigenvalues of the Hamiltonian problem, as induced by the $\mathcal{PT}$-symmetric terms.

In particular, it is interesting to examine the results for the continuum limit, where for both the sine-Gordon and the ϕ^4 models, the eigenvectors of the linearization are well known [41]. In the case of the sine-Gordon $w_0^{(0)} = (1/2)\mathrm{sech}(x - x_0)$, while the continuous spectrum consists of the nondecaying eigenfunctions $w_0^{(k)} = e^{ik(x-x_0)}[k + i\tanh(x - x_0)]/(k + i)$. A direct inspection of Eq. (9), given the (even) parity of the square modulus of these eigenvectors and the odd nature of the gain and loss profile, naturally leads to $\lambda_1 = 0$ (when the kink is placed exactly at the interface between gain and loss regions). Thus, we do *not* expect a leading-order correction to the relevant eigenvalues. Similar conclusions can be straightforwardly inferred in the ϕ^4 model, due to the definite parity of the eigenvectors therein [42], as well. In fact, as we argue below, this is a general conclusion that our numerics support as being true to all orders for the continuum, infinite domain PDE problem, for a kink centered exactly between the gain and the loss regions (for further comments on kinks centered on the gain side or on the lossy side, see below).

We now provide a rigorous estimate on the potential size of any unstable eigenvalues in this system. In particular, we show that while the eigenvalues may be unstable, their real part is at most $O(\epsilon)$ (i.e., the size of the $\mathcal{PT}$-symmetric perturbation). Indeed, consider the linearized problem in the form

$$w_{tt} - \gamma(x)w_t + \hat{C}w = 0. \tag{10}$$

Recall that $\hat{C} \geqslant 0$ by Sturm-Liouville theory since the ground state is the positive function u_0' (see also the discussion above, with u_0 denoting the kink and the prime indicating derivative with respect to x). Then, taking a dot product with w_t in (10), we obtain

$$\partial_t(\|w_t\|^2 + \langle \hat{C}w, w\rangle) = 2\int \gamma(x)|w_t(t,x)|^2 dx.$$

Since $\langle \hat{C}w, w\rangle \geqslant 0$, integrating the last identity in t yields (note that $|\gamma(x)| \leqslant K\epsilon$, where $K = \max_{x>0} xe^{-x^2/2}$)

$$\|w_t(t)\|^2 \leqslant 2\int_0^t \int |\gamma(x)||w_s(s,x)|^2 dx\, ds$$
$$\leqslant 2K\epsilon \int_0^t \|w_s(s)\|^2 ds.$$

By Gronwall's inequality [43], we can straightforwardly infer that

$$\|w_t(t)\|^2 \leqslant \|w_t(0)\|^2 e^{2Kt\epsilon}.$$

Thus, for the potentially unstable eigenvalue λ, which generates an unstable solution in the form $w = e^{\lambda t} f(x)$, we have the bound $e^{2t\lambda_r}\|f\|^2 \leqslant e^{2Kt\epsilon}\|f\|^2$, for all $t > 0$, hence the real part λ_r of the relevant eigenvalues (corresponding to the instability growth rate) satisfies $\lambda_r \leqslant K\epsilon$. We now turn to numerical computations to explore the nature of the linearization spectrum.

III. NUMERICAL RESULTS

For practical (numerical) reasons, but also given that they are models of interest in their own right (see. e.g., [36,37] and references therein), we will present our conclusions in the context of the discrete variant of the Klein-Gordon equations of the form

$$\ddot{u}_n = \frac{1}{\Delta x^2}(u_{n+1} + u_{n-1} - 2u_n) + f(u_n) + \gamma_n \dot{u}_n. \tag{11}$$

More specifically, we will consider the case of finite Δx, typically of $O(1)$ ($\Delta x = 1$ unless stated otherwise; in fact, it will be set to unity for all the figures except for Fig. 4) and in the process, we will also explain how the limit of $\Delta x \to 0$, as well as the distinct from it infinite lattice (but with finite Δx) limit are approached.

A feature which is of interest in nonlinear dynamical lattices of the form of Eq. (11) is the existence of two distinct kink solutions, one centered on a site (having a site with $u_n = \pi$ in the sG model and a site with $u_n = 0$ in the ϕ^4 case) which is unstable, and one centered between two adjacent sites, which is dynamically stable in the Hamiltonian limit [37]. The difference between these two solutions is the celebrated Peierls-Nabarro barrier [36]. We start by considering the site-centered (SC) solutions in Fig. 1. We will typically fix in what follows the strength of our perturbation to $\epsilon = 0.1$, although we have tested the validity of the conclusions for other values of ϵ as well. In Fig. 1, the results of the spectral analysis of Eq. (5) are given by presenting the spectral plane (λ_r, λ_i) of the eigenvalues $\lambda = \lambda_r + i\lambda_i$. In the Hamiltonian

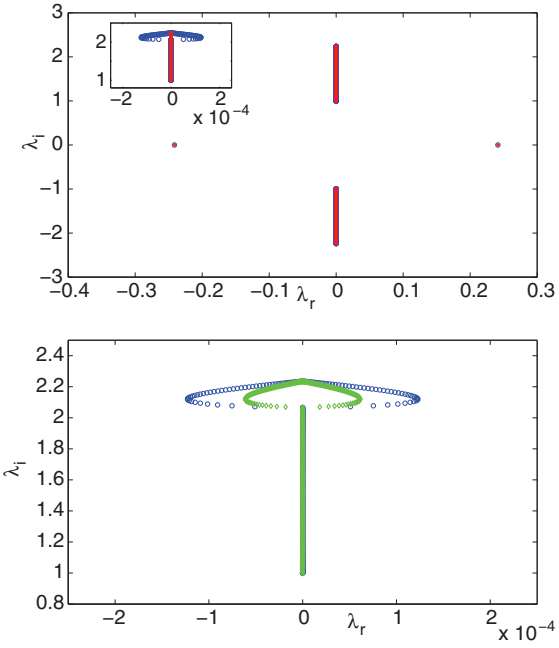

FIG. 1. (Color online) The top panel shows the spectral plane (λ_r, λ_i) of the eigenvalues $\lambda = \lambda_r + i\lambda_i$ for the linearization around the site-centered kink at $n = 0$, for the discrete case with $\Delta x = 1$, and with perturbation strength $\epsilon = 0.1$ (blue circles: for comparison the $\epsilon = 0$ case is shown by red stars) in the sine-Gordon model. The top panel has an inset which is a blowup of the top part of the continuous spectrum. Here, the lattice consists of $N = 399$ sites, while in the bottom panel the case of $N = 399$ (blue circles) is compared to that of $N = 799$ (green diamonds). In the regions where the green diamonds of the bottom panel and the red stars of the top panel coincide with the blue circles, the latter are not shown.

limit of $\epsilon = 0$, this spectrum possesses a real eigenvalue pair (denoting the instability of the SC configuration) and a continuous spectrum following the dispersion relation $\lambda = \pm i\sqrt{1 + (4/\Delta x^2)\sin^2(k\Delta x/2)}$ and extending over the interval $\pm[1, \sqrt{1 + (4/\Delta x^2)}]$ on the imaginary axis. The top panel of the figure shows the spectrum for a lattice of $N = 399$ sites. The real eigenvalue is preserved (in fact, unchanged from the Hamiltonian limit) and so is the continuous spectrum, except for the case of wave numbers close to $k = \pi/\Delta x$ near the top of the spectrum. Even this feature, however, is only an artifact of the finite size of the lattice, as is shown in the bottom panel. The latter shows the case of $N = 399$ versus that of $N = 799$ sites (at fixed $\Delta x = 1$). In the latter, the relevant effect weakens, indicating that it will disappear in the limit of the infinite lattice (of fixed spacing). Hence, this suggests that the solution centered at the interface between gain and loss experiences no effect in its stability in the infinite lattice discrete limit. This, in turn, is suggestive that a similar insensitivity to $\mathcal{PT}$ symmetry should be present in the continuum limit (see also the discussion below and the arguments above).

In the case of Fig. 2, we examine what happens if we displace the kink. Here, instead of centering it at $n = 0$, we select to center it on a gain site, and more specifically at $n = 3$. It is straightforward to see that if centered on the lossy side, the spectrum would be a mirror image with respect to the imaginary axis. The top panel of the figure for $N = 799$

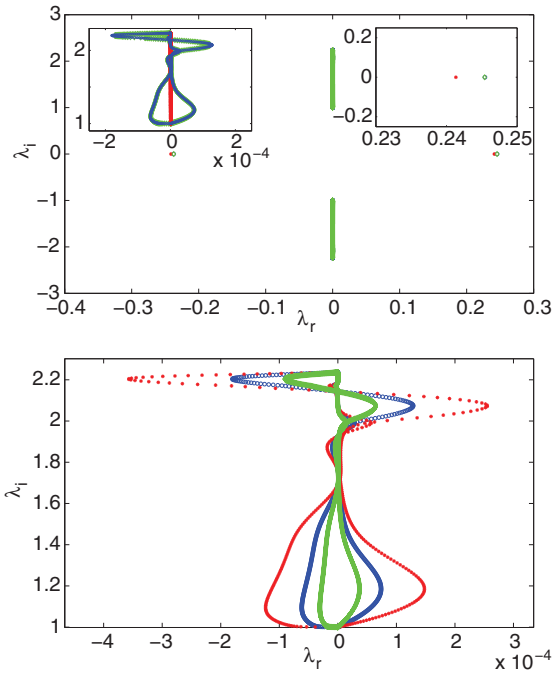

FIG. 2. (Color online) The top panel shows the comparison for $\epsilon = 0.1$, $N = 799$ of the spectral plane of a site-centered kink at $n = 3$ between numerics (blue circles) and theory of Eqs. (6)–(9) (green diamonds). The case of $\epsilon = 0$ is shown by red stars as a benchmark. The insets show details of the continuous spectrum (left) and the positive real part of the point spectrum (right). The bottom panel shows a blowup of the upper band of the continuous spectrum for $N = 399$ (red stars), $N = 799$ (blue circles), and $N = 1599$ (green diamonds).

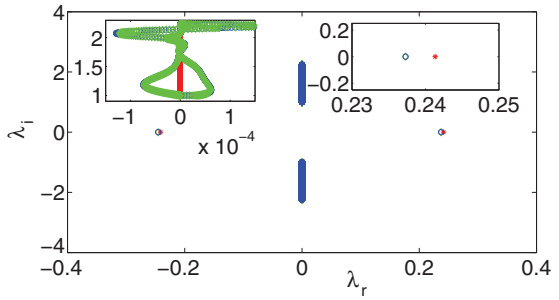

FIG. 3. (Color online) For $N = 799$, the spectrum of a kink centered at $n = -3$ is given for $\epsilon = 0.1$ (blue circles). The continuous spectrum is the mirror image of the case centered at $n = 3$. The analytical prediction based on Eqs. (6)–(9) is given by the green diamonds, while the case of $\epsilon = 0$ is given for reference by the red stars. The insets show details of the continuous (left) and point (right) spectrum.

compares the numerically observed shifts in the eigenvalues (blue circles) with the semianalytical prediction obtained on the basis of Eqs. (6)–(9) (green diamonds). It can be seen that the agreement is *excellent*. For comparison, the case with $\epsilon = 0$ is also shown by red stars. The bottom panel illustrates, for this case as well, the effect of tending towards the infinite lattice at fixed spacing. The red stars are for $N = 399$, the blue circles for $N = 799$, and the green diamonds for $N = 1599$, clearly attesting to the finite nature of this effect. Thus, for the infinite lattice, such bifurcations appear to be suppressed. We should note on the other hand that the position of the point spectrum (real, in this case) eigenvalue does not shift as N changes.

In the case of Fig. 3, we showcase what happens when considering a kink centered at $n = -3$ instead of $n = +3$. The reference of $\epsilon = 0$ (red stars) indicates that the real eigenvalues move in this case to the left (as opposed to the right in Fig. 2). This point spectrum as well as the continuous spectrum (of blue circles for $\epsilon = 0.1$) is once again captured very accurately by the analytical expressions of Eqs. (6)–(9), evaluated at the unperturbed limit w_0.

We now turn to the examination of the stable (in the Hamiltonian limit) kinks which are intersite centered (IC). Figure 4 shows the IC kink centered at 0.5, with $N = 799$ sites. It is interesting to note that, in this case, the eigenvalue which in the continuum limit is associated with translation (and in that limit is at $\lambda = 0$) is imaginary and hence the real contribution of Eq. (9) renders it complex. In fact, we find that a simple (approximate) evaluation based on the continuum eigenvector $w_0 \sim \mathrm{sech}(x - 0.5)$ yields from Eq. (9) a correction of $\approx 0.105\epsilon$, which is in very reasonable agreement with the observation of Fig. 4. Another interesting feature of the figure is the fact that for $\Delta x = 1$, the mode of the band edge [with an eigenvector which is $\sim \tanh(x - x_0)$] has bifurcated into an internal mode of the discrete sine-Gordon system [37]. This internal mode [given that $\tanh^2(y) = 1 - \mathrm{sech}^2(y)$] is found to bifurcate in the *opposite* direction, moving into the left half of the complex spectral plane, as shown in the figure.

The bottom panel of Fig. 4 shows another interesting feature, examining essentially how the continuum limit of the problem is approached for the case of a kink centered

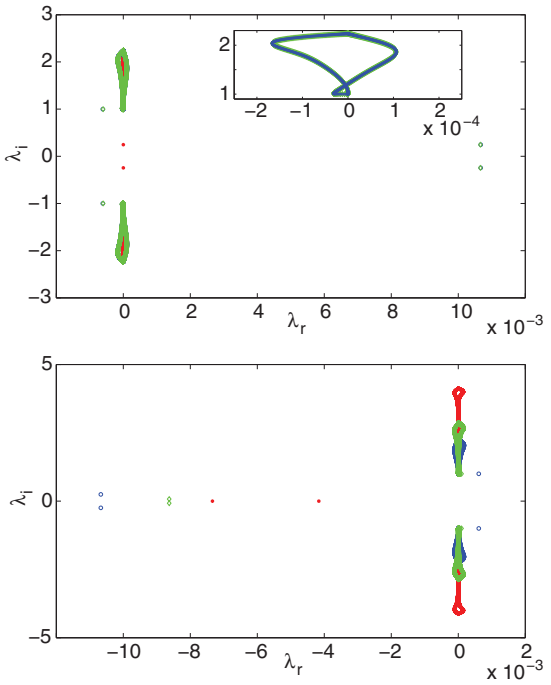

FIG. 4. (Color online) The top panel shows the case of the intersite-centered kink at $n = 0.5$ for $\epsilon = 0.1$ (blue circles) versus the corresponding prediction of Eq. (9) (green diamonds). The inset shows a zoom of the upper branch of the continuous spectrum. The red stars denote the case of $\epsilon = 0$. The bottom panel, in turn, shows three cases for $n = -0.5$, namely, those of $N = 799$ and $\Delta x = 1$ (blue circles), $N = 1067$ with $\Delta x = 0.75$ (green diamonds), and $N = 1599$ with $\Delta x = 0.5$ (red stars).

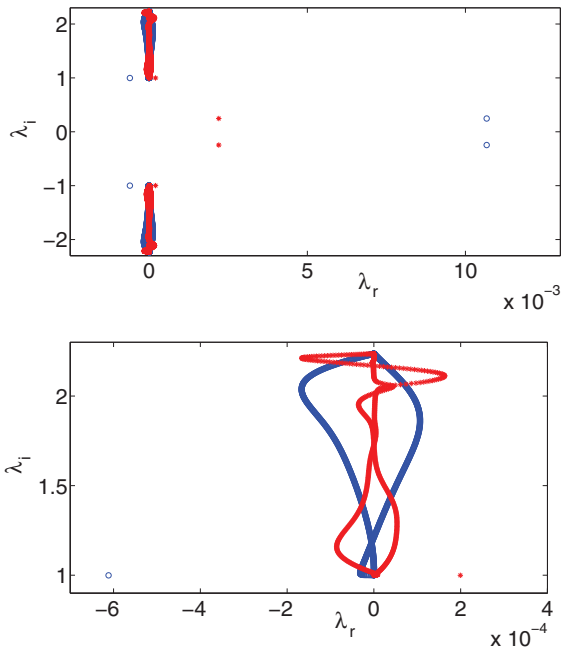

FIG. 5. (Color online) The top panel shows the full spectrum for IC kinks centered at $n = 0.5$ (blue circles) and $n = 3.5$ (red stars). A detail of the top panel showing the internal mode bifurcating from the band edge and the continuous spectrum is shown in the bottom panel.

at $n = -0.5$. For $N = 799$ and $\Delta x = 1$, the spectrum (as expected) is the mirror image of that shown for $n = 0.5$ in the top panel. However, there are two more cases shown in the panel, namely, $N = 1067$ with $\Delta x = 0.75$ (green diamonds) and $N = 1599$ with $\Delta x = 0.5$ (red stars). The choices are made so that the total size of the domain remains essentially the same. What can be clearly seen is that the point spectrum eigenvalues approach the imaginary axis. In particular, the translational eigenvalue tends to zero (notice that the relevant eigenvalue moves also from complex to real, as the continuum limit is approached). The mode bifurcating from the bottom of the band edge can no longer be discerned for the smaller values of Δx. Finally, the continuous spectrum aligns along the imaginary axis with the only source of instability arising due to the large wave numbers (smaller wavelengths) which are being "advected" as the limit is approached, towards infinity. This is another strong indication that in the limit of $\Delta x \to 0$ and $N \to \infty$, no instability is anticipated in the model and the kinks should be dynamically robust.

One feature which is also worth noting is that the bifurcation of the internal modes may nontrivially depend on the specific position of the kink. In particular, in Fig. 5, the case of an IC kink centered at $n = 0.5$ (blue circles) is compared to that of one centered at $n = 3.5$ (red stars). The top panel shows the full diagram, indicating that the predominant instability due to the translational mode weakens [as expected due to the rapid decay of $\gamma(x)$] as we go deeper into the gain side. Yet, it is more interesting to notice the far more complex details of the bottom panel showcasing significant differences between the continuous spectrum of the two, which perhaps merit further investigation. However, importantly, we should mention that the internal mode that we saw as bifurcating from the band edge [37] and moving to the left half plane in Fig. 4, is now moving to the right for the IC kink centered at $n = 3.5$.

We should highlight one more possibility here. Up until now, we have been focusing on a gain and loss profile that is symmetric around an origin, which happens to be a site of the underlying lattice. In this case, to create a $\mathcal{PT}$-symmetric domain, we have selected an odd number of sites. However, an additional possibility exists, whereby we choose the domain to have an even number of sites, such as $N = 800$ in the case of Fig. 6, and have the domain centered between two adjacent sites of our grid, namely, at 0.5. In such a setting, instead of the SC mode being "symmetric" when centered at the origin, and the IC mode being "asymmetric" when centered at 0.5, the roles are reversed. In particular, SC modes are always asymmetric (and hence will always feature $\mathcal{PT}$-symmetry induced bifurcations of their corresponding eigenvalues, except for the infinite domain, continuum limit case where such bifurcations should vanish for a kink centered at the origin). To showcase a feature of this sort, we selected the IC mode centered at $n = 0.5$ for $N = 799$ (blue circles) and $N = 800$ (green diamonds) for $\epsilon = 0.1$. While the circles represent the asymmetric case of Fig. 4, it is clear that the diamonds are analogous to the case of Fig. 1, indicating that the symmetry yields the absence of any bifurcations, aside from the finite size effect arising at the top of the band.

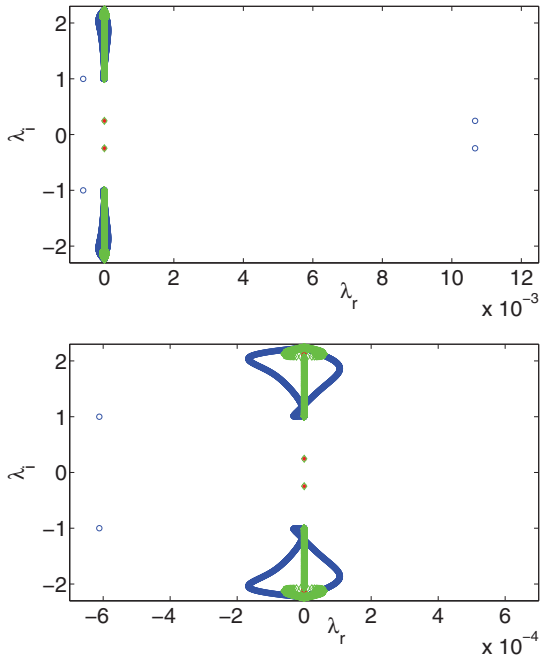

FIG. 6. (Color online) The difference between an intersite-centered kink for the asymmetric case for $N = 799$ (blue circles) and the symmetric case of $N = 800$ (green diamonds) for $\epsilon = 0.1$ (see also the text). The bottom panel shows a blowup of the continuous spectrum in the two cases.

We would also like to point out that these results are not restricted to the case of the sine-Gordon model. As

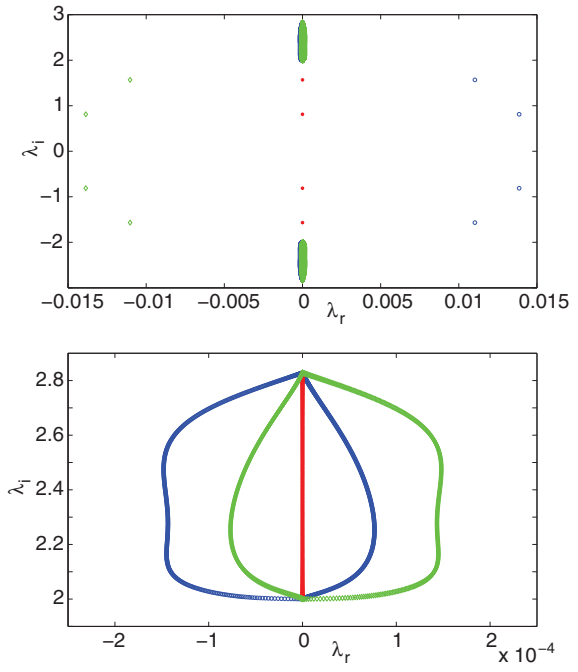

FIG. 7. (Color online) The top panel shows the results of a linearization around the ϕ^4 kink for $\epsilon = 0.1$, $N = 799$, and two kinks centered at $n = 0.5$ (blue circles) and $n = -0.5$ (green diamonds). The bottom panel shows a blowup of the top panel clearly showcasing the continuous spectrum of the model.

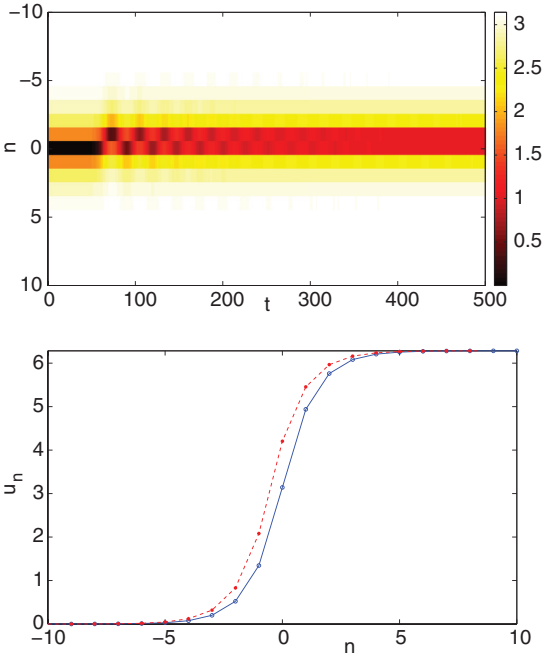

FIG. 8. (Color online) The top panel shows the space (n) -time (t) evolution of the field $|u_n - \pi|$ for a site-centered kink at $n = 0$, for a $N = 799$ site lattice with $\epsilon = 0.1$. Notice the motion towards an intersite-centered kink centered at $n = -0.5$, clearly illustrated also in the initial (blue circles) and final (red stars) snapshots of the configuration (in the bottom panel).

an example of the generality of the relevant results, in Fig. 7, we have considered both the kink centered at $n = 0.5$ and that centered at $n = -0.5$ (blue circles and green diamonds, respectively, clearly showing the mirror nature of the relevant spectra) for a ϕ^4 model with $N = 799$, $\epsilon = 0.1$, and $\Delta x = 1$. A distinctive feature of this case concerns the presence of an additional internal mode even in the continuum limit [where its eigenvalue is $\lambda = \pm i\sqrt{3}$ and its eigenvector $\sim$sech(x) tanh(x)]. Interestingly, and as can be verified also by Eq. (9), the bifurcation of both the translational mode and this continuum internal mode occur in the same direction, i.e., to the right-half plane for $n = 0.5$ and to the left-half plane for the case of $n = -0.5$. Nevertheless, even in that case, as shown in the blowup of the bottom panel of the figure illustrating the continuous spectrum, the kink in the ϕ^4 model is still unstable, although as discussed earlier this instability will disappear in the infinite domain limit (either for Δx finite or in the continuum infinite domain limit where also $\Delta x \to 0$).

Finally, in order to corroborate the spectral conclusions given above, we have examined some select dynamical evolution simulations. In Fig. 8, we describe the evolution of a site-centered kink at $n = 0$ for the sine-Gordon model, with $N = 799$ and $\epsilon = 0.1$. The field $|u_n - \pi|$ is shown which places on equal footing the asymptotic steady states of 0 and 2π and shows the kink as a dip (from a background of π towards 0). It can be clearly seen that the site-centered kink, spontaneously perturbed by a small-amplitude random (uniformly distributed) noise rearranges itself towards a stable

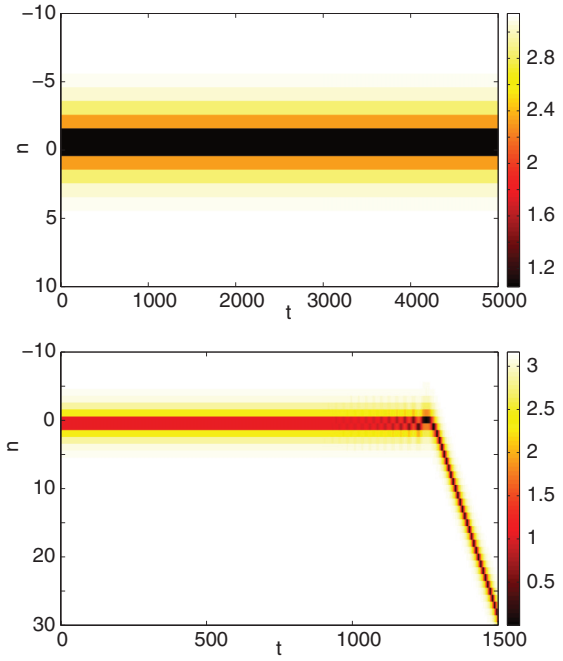

FIG. 9. (Color online) The top panel shows the space-time evolution of an intersite-centered kink initially at $n = -0.5$, which appears to be dynamically unchanged with the numerical reporting horizon of this run. The bottom panel shows an oscillatory instability (i.e., instability arising in parallel to oscillations; see the increasing amplitude "spots" emerging around $t = 1000$) developing for a kink initially centered at $n = 0.5$ and consequently "expelled" (i.e., forced to move) towards the gain side.

intersite-centered kink. However, notice (we have observed this to be systematic and it is also in line with similar observations in nonlinear Schrödinger-type (NLS) models [44]) that the stable intersite-centered kink towards which the dynamics evolves is the one centered at the "lossy" side and, in particular, at $n = -0.5$. The snapshot of the bottom panel confirms this evolution. On the other hand, we have observed (data not shown) that if the random perturbation (or a deterministic one along the direction of translation) moves the kink towards the gain side, then the kink starts traveling (in the ultimately decelerated way described in Ref. [36]), rather than settling to an IC waveform. This feature is also reminiscent of the behavior observed in the case of the dark solitary waves of the NLS.

On the other hand, in Fig. 9, we present the evolution of two IC kinks. The first is centered at $n = -0.5$ (the outcome of the evolution of Fig. 8), which according to Fig. 4 is unstable but apparently the development of the instability takes longer to evolve than the already very long times of the simulation due to the weakness of the corresponding growth rate. The second is centered at $n = 0.5$ bearing a stronger oscillatory instability (due to a complex eigenvalue pair) according to Fig. 5. Indeed, we observe precisely the manifestation of a corresponding oscillatory growth, leading eventually to the kink being expelled towards the gain side and towards a traveling (and eventually decelerating) wave.

IV. CONCLUSIONS AND FUTURE CHALLENGES

In this work, we have introduced a class of $\mathcal{PT}$-symmetric models in the context of nonlinear Klein-Gordon field theories. We have focused more specifically on the kinklike steady states. Our analysis provided not only a class of models, but also a way to assess the spectral features induced by the presence of such $\mathcal{PT}$-symmetric perturbations. It was argued that for solutions symmetrically placed at the interface of the gain and the loss regions, no stability modifications are present. However, such modifications may arise when there is an asymmetry. This asymmetry can, in principle, exist even in the continuous limit, although we have mostly focused on the one induced by nonlinear dynamical lattices (i.e., the discretized form of the PDE) and their onsite or intersite solutions. The asymmetry towards the lossy side has been observed to be beneficial for stability purposes, while that towards the gain side to be typically unstable. In addition, a wide range of continuous spectrum finite size induced effects have been presented, but no detailed explanation thereof has been offered.

Naturally, since this is a field at a nascent stage, a wide range of questions remain open. On the one hand, understanding the differences between a finite and an infinite lattice, as highlighted above, has been singled out as an important problem. Notice that recent studies illustrate the relevance of such an understanding even in NLS-type dynamical lattices. On the other hand, perhaps even more pressing questions might concern the fate of solutions which are genuinely time dependent. Examples of the latter kind consist of, e.g., the traveling waves or the breather states. Traveling waves are unlikely to retain their character given the spatial inhomogeneity incurred within the domain, yet may have interesting scattering properties. What one may expect, at least in the perhaps simpler, as regards traveling properties continuum problem, also in line with the observations of Fig. 9, is the following. For a kink on the gain side, the $\mathcal{PT}$-symmetric term causes it to accelerate before the $\mathcal{PT}$ effect decays away and we are left with a higher speed kink traveling to the right. For a kink on the lossy side, if the speed is weak, then the $\mathcal{PT}$-symmetric effect may ground the kink to a complete halt. If, however, the speed is sufficiently high so as to overcome the $\mathcal{PT}$-induced potential, then we will have a kink asymptotically propagating on the left side. As regards the breathers, on the other hand, they may be especially interesting to examine since, in analogy with NLS-type cases, they may be likely to exist if suitably produced; for instance, one might expect that again it may be relevant to balance the gain and loss pattern and center such breathers at the origin. These are among the canonical themes for future investigations and will be explored in future publications.

ACKNOWLEDGMENTS

The work of D.J.F. was partially supported by the Special Account for Research Grants of the University of Athens. A. Saxena is supported by the US Department of Energy. P.G.K. is supported by Grants No. NSF-DMS-0806762 and No. NSF-CMMI-1000337, as well as by the US AFOSR under Grant No. FA9550-12-1-0332, the Alexander von Humboldt Foundation, and the Binational Science Foundation (Grant No. 2010239).

[1] C. M. Bender and S. Boettcher, Phys. Rev. Lett. **80**, 5243 (1998).
[2] C. M. Bender, Rep. Prog. Phys. **70**, 947 (2007).
[3] C. M. Bender, S. Boettcher, and P. N. Meisinger, J. Math. Phys. **40**, 2201 (1999).
[4] Z. H. Musslimani, K. G. Makris, R. El-Ganainy, and D. N. Christodoulides, Phys. Rev. Lett. **100**, 030402 (2008).
[5] K. G. Makris, R. El-Ganainy, D. N. Christodoulides, and Z. H. Musslimani, Phys. Rev. Lett. **100**, 103904 (2008).
[6] A. Guo, G. J. Salamo, D. Duchesne, R. Morandotti, M. Volatier-Ravat, V. Aimez, G. A. Siviloglou, and D. N. Christodoulides, Phys. Rev. Lett. **103**, 093902 (2009).
[7] C. E. Ruter, K. G. Makris, R. El-Ganainy, D. N. Christodoulides, M. Segev, and D. Kip, Nat. Phys. **6**, 192 (2010).
[8] A. Regensburger, C. Bersch, M.-A. Miri, G. Onishchukov, D. N. Christodoulides, and U. Peschel, Nature (London) **488**, 167 (2012).
[9] A. Ruschhaupt, F. Delgado, and J. G. Muga, J. Phys. A: Math. Gen. **38**, L171 (2005).
[10] M. Hiller, T. Kottos, and A. Ossipov, Phys. Rev. A **73**, 063625 (2006).
[11] H. Ramezani, T. Kottos, R. El-Ganainy, and D. N. Christodoulides, Phys. Rev. A **82**, 043803 (2010).
[12] A. A. Sukhorukov, Z. Xu, and Yu. S. Kivshar, Phys. Rev. A **82**, 043818 (2010).
[13] M. C. Zheng, D. N. Christodoulides, R. Fleischmann, and T. Kottos, Phys. Rev. A **82**, 010103(R) (2010).
[14] E. M. Graefe, H. J. Korsch, and A. E. Niederle, Phys. Rev. Lett. **101**, 150408 (2008).
[15] E. M. Graefe, H. J. Korsch, and A. E. Niederle, Phys. Rev. A **82**, 013629 (2010).
[16] Z. Lin, H. Ramezani, T. Eichelkraut, T. Kottos, H. Cao, and D. N. Christodoulides, Phys. Rev. Lett. **106**, 213901 (2011).
[17] K. Li and P. G. Kevrekidis, Phys. Rev. E **83**, 066608 (2011).
[18] S. V. Dmitriev, S. V. Suchkov, A. A. Sukhorukov, and Yu. S. Kivshar, Phys. Rev. A **84**, 013833 (2011).
[19] S. V. Suchkov, B. A. Malomed, S. V. Dmitriev, and Yu. S. Kivshar, Phys. Rev. E **84**, 046609 (2011).
[20] R. Driben and B. A. Malomed, Opt. Lett. **36**, 4323 (2011).
[21] R. Driben and B. A. Malomed, Europhys. Lett. **96**, 51001 (2011).
[22] F. Kh. Abdullaev, V. V. Konotop, M. Ögren, and M. P. Sørensen, Opt. Lett. **36**, 4566 (2011).
[23] N. V. Alexeeva, I. V. Barashenkov, A. A. Sukhorukov, and Yu. S. Kivshar, Phys. Rev. A **85**, 063837 (2012).
[24] A. E. Miroshnichenko, B. A. Malomed, and Yu. S. Kivshar, Phys. Rev. A **84**, 012123 (2011).
[25] F. Kh. Abdullaev, Y. V. Kartashov, V. V. Konotop, and D. A. Zezyulin, Phys. Rev. A **83**, 041805(R) (2011).
[26] D. A. Zezyulin, Y. V. Kartashov, and V. V. Konotop, Europhys. Lett. **96**, 64003 (2011).
[27] M. Duanmu, K. Li, R. L. Horne, P. G. Kevrekidis, and N. Whitaker, Philos. Trans. R. Soc., A **371**, 20120171 (2013).
[28] T. Dauxois and M. Peyrard, *Physics of Solitons* (Cambridge University Press, Cambridge, UK, 2006).
[29] R. K. Dodd, J. C. Eilbeck, J. D. Gibbon, and H. C. Morris, *Solitons and Nonlinear Wave Equations* (Academic, New York, 1983).
[30] M. Remoissenet, *Waves Called Solitons* (Springer, Berlin, 1999).
[31] J. Schindler, A. Li, M. C. Zheng, F. M. Ellis, and T. Kottos, Phys. Rev. A **84**, 040101 (2011).
[32] H. Ramezani, J. Schindler, F. M. Ellis, U. Günther, and T. Kottos, Phys. Rev. A **85**, 062122 (2012).
[33] C. M. Bender, B. J. Berntson, D. Parker, and E. Samuel, Am. J. Phys. **81**, 173 (2013).
[34] N. Lazarides and G. P. Tsironis, Phys. Rev. Lett. **110**, 053901 (2013).
[35] A. M. Shalaby, arXiv:0912.0304.
[36] M. Peyrard and M. D. Kruskal, Physica D (Amsterdam) **14**, 88 (1984); P. G. Kevrekidis and M. I. Weinstein, *ibid*. **142**, 113 (2000).
[37] P. G. Kevrekidis and C. K. R. T. Jones, Phys. Rev. E **61**, 3114 (2000); N. J. Balmforth, R. V. Craster, and P. G. Kevrekidis, Physica D (Amsterdam) **135**, 212 (2000).
[38] J. Cuevas, L. Q. English, P. G. Kevrekidis, and M. Anderson, Phys. Rev. Lett. **102**, 224101 (2009).
[39] L. Q. English, F. Palmero, P. Candiani, J. Cuevas, R. Carretero-González, P. G. Kevrekidis, and A. J. Sievers, Phys. Rev. Lett. **108**, 084101 (2012).
[40] G. Sh. Guseinov and G. Oturanc, Turkish J. Math. **21**, 409 (1997).
[41] M. B. Fogel, S. E. Trullinger, A. R. Bishop, and J. A. Krumhansl, Phys. Rev. B **15**, 1578 (1977).
[42] T. Sugiyama, Prog. Theor. Phys. **61**, 1550 (1979).
[43] T. H. Gronwall, Ann. Math. **20**, 292 (1919).
[44] V. Achilleos, P. G. Kevrekidis, D. J. Frantzeskakis, and R. Carretero-González, Phys. Rev. A **86**, 013808 (2012); arXiv:1208.2445.
[45] D. E. Pelinovsky, P. G. Kevrekidis, and D. J. Frantzeskakis, Europhys. Lett. **101**, 11002 (2013).